ISSN 2176-5480

22nd International Congress of Mechanical Engineering (COBEM 2013)
November 3-7, 2013, Ribeirão Preto, SP, Brazil

A STUDY ON HIGH-ORDER SPECTRAL DIFFERENCE METHOD FOR COMPRESSIBLE FLOW SIMULATIONS

Fábio Mallaco Moreira
Universidade Estadual de Campinas, Campinas, Brazil
fabiom91@gmail.com

Carlos Breviglieri
Instituto Tecnológico de Aeronáutica, São José dos Campos, SP, Brazil
carbrevi@gmail.com

João Luiz F. Azevedo
Instituto de Aeronáutica e Espaço, São José dos Campos, SP, Brazil
joaoluiz.azevedo@gmail.com

Abstract. *High order methods are necessary on the analysis of complex flows to improve the numerical solution where a specific accuracy needs to be met by the spatial discretization scheme. The primary interest of the paper is to investigate the proper solution accuracy and resolution of the Spectral Difference method for compressible aerodynamic flows. The scheme is implemented in an unstructured grid, two dimensional framework for the solution of the Euler equations and allows for reconstructions up to 6th-order accurate.*

Keywords: *Spectral Difference; Spectral Volume; High-order schemes; Unstructured meshes; Aerodynamic applications*

1. INTRODUCTION

High order methods are necessary on the analysis of complex flows to reduce the number of mesh elements one would otherwise need if using traditional second-order schemes. Assessment of solution reliability in such cases may also require that a specified solution accuracy be met by the spatial discretization scheme. The method considered in this work was developed as an alternative to the discontinuous Galerkin, k-exact, ENO/WENO and Spectral Volume (SV) high-order schemes. Their common objective is to allow the implementation of a simpler and more efficient scheme, while still achieving high-order spatial accuracy. The spectral difference (SD) method is implemented in an unstructured, two dimensional Euler framework. The implemented scheme allows for 2nd, 3rd and 4th-order accurate solutions, which use the Roe Riemann solver as the basic numerical flux scheme.

The SFV method, as developed by Wang (2002) circa 2002, was further extended to handle hyperbolic systems, two and three dimensions, smooth and discontinuous flow solutions. This method was originally incorporated by the authors into a 2-D finite volume solver due to its similar underlying structure (Breviglieri *et al.*, 2010). However, the SV method, at its current state, supports only triangular mesh elements. This proves to be a drawback if one is concerned with viscous flows, mainly due to the boundary layer discretization, where quadrilateral elements are better suited for the gradients discretization. The SD scheme by Liu *et al.* (2006) is very popular among high-order CFD research groups throughout the world and shares many of the SV scheme attributes, as previously described, only that its formulation is suited for quadrilateral unstructured meshes.

The present work represents an effort to evaluate the SD method as an alternate high-order method for the applications of interest to the authors, namely external compressible aerodynamic flows. Moreover, the CFD solver developed by the authors and used in the present work has been verified and validated previously (Breviglieri *et al.*, 2010; Breviglieri and Azevedo, 2012). The paper is organized as follows. First, the numerical formulation of the SD method for the Euler equations in 2-D is presented. The formal order of accuracy of the SD scheme is measured and the final section presents numerical results for well-known literature test cases.

2. SPECTRAL DIFFERENCE METHOD

The Spectral Difference formulation in the present work considers the unsteady compressible 2-D Euler equations in conservative form

$$\frac{\partial Q}{\partial t} + \frac{\partial E}{\partial x} + \frac{\partial F}{\partial y} = 0 \,, \tag{1}$$

ISSN 2176-5480

where Q is the vector of conserved variables, E and F are the flux vectors in the Cartesian coordinates. The implementation follows the formulation presented in Wang *et al.* (2007) and May and Jameson (2006). The numerical solver, in which the SD method is implemented, was originally developed in a Finite Volume context. The SD method employs a Finite Difference like scheme and it represents a different approach to the solver programming and algorithm considerations. For instance, to achieve an efficient implementation, all elements in the physical domain (x, y) are transformed into a unit square element in the computational domain. Such transformation can be written as

$$\begin{pmatrix} x \\ y \end{pmatrix} = \sum_{i=1}^{K} M_i(\xi, \eta) \begin{pmatrix} x_i \\ y_i \end{pmatrix} , \tag{2}$$

where K is the number of points used to define the physical element, (x_i, y_i) are the Cartesian coordinates of those points, and $M_i(\xi, \eta)$ are the shape functions of the geometric transformation. The metrics and the Jacobian of the transformation can be computed in a pre-processing step and kept in memory given the stationary aspect of the problems here considered. The governing equations in the physical domain are then transferred into the computation domain, and can be rewritten as

$$\frac{\partial \tilde{Q}}{\partial t} + \frac{\partial \tilde{E}}{\partial x} + \frac{\partial \tilde{F}}{\partial y} = 0 \, , \tag{3}$$

where $\tilde{Q} = |J| \cdot Q$ and

$$\begin{pmatrix} \tilde{E} \\ \tilde{F} \end{pmatrix} = |J| \begin{pmatrix} \xi_x & \xi_y \\ \eta_x & \eta_y \end{pmatrix} \begin{pmatrix} E \\ F \end{pmatrix} . \tag{4}$$

In the standard element, two sets of points are defined, namely the solution points (SP) and the flux points (FP), illustrated in Fig. 1. In order to construct a degree $(N-1)$ polynomial to achieve high-order resolution, solution at N points are required. The solution points in 1-D are chosen to be the Gauss points defined by

$$X_s = \frac{1}{2}\left[1 - \cos\left(\frac{2s-1}{2N} \cdot \pi\right)\right], s = 1, 2, \cdots, N. \tag{5}$$

The flux points are selected to be the Gauss-Lobatto points given by

$$X_{s+\frac{1}{2}} = \frac{1}{2}\left[1 - \cos\left(\frac{s}{N} \cdot \pi\right)\right], s = 0, 1, \cdots, N. \tag{6}$$

Using the solution at N solution points, a degree $(N-1)$ polynomial can be built using the following Lagrange basis defined as

$$h_i(X) = \prod_{s=0, s\neq i}^{N} \left(\frac{X - X_s}{X_i - X_s}\right) \tag{7}$$

similarly, using the fluxes at $(N+1)$ flux points, a degree N polynomial can be built for the flux using a similar Lagrange basis defined as

$$l_{i+\frac{1}{2}}(X) = \prod_{s=0, s\neq i}^{N} \left(\frac{X - X_{s+\frac{1}{2}}}{X_{i+\frac{1}{2}} - X_{s+\frac{1}{2}}}\right) . \tag{8}$$

The reconstructed solution for the conserved variables in the standard element is just the tensor products of the two one-dimensional polynomial,

$$Q(\xi, \eta) = \sum_{j=1}^{N}\sum_{i=1}^{N} \frac{\tilde{Q}_{i,j}}{|J_{i,j}|} h_i(\xi) \cdot h_j(\eta) \, . \tag{9}$$

Similarly, the reconstructed flux polynomials take the following form

$$\tilde{E}(\xi, \eta) = \sum_{j=1}^{N}\sum_{i=0}^{N} \tilde{E}_{i+\frac{1}{2},j} l_{i+\frac{1}{2}}(\xi) \cdot h_j(\eta), \tag{10}$$

$$\tilde{F}(\xi, \eta) = \sum_{j=0}^{N}\sum_{i=1}^{N} \tilde{F}_{i,j+\frac{1}{2}} h_i(\xi) \cdot l_{j+\frac{1}{2}}(\eta). \tag{11}$$

ISSN 2176-5480

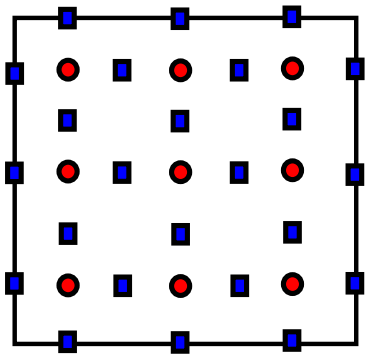

Figure 1. Possible flux points (blue squares) and solution points (red circles) distribution for the SD method.

The reconstructed fluxes are only element-wise continuous, but discontinuous across cell interfaces. For the inviscid flux, a Riemann solver is employed to compute a common flux at interfaces to ensure conservation and stability. In the present work, the Roe approximate Riemann solver is considered. The numerical flux introduces the artificial dissipation and upwind characteristic to the method.

In order to compute the inviscid flux derivatives the SD method computes the conservative variables at the flux points. The inviscid fluxes are then updated followed by the numerical flux calculations. The derivatives of the fluxes are computed at the solution points using the derivatives of Lagrange operators l as

$$\begin{aligned} \left(\frac{\partial \tilde{E}}{\partial \xi} \right)_{i,j} &= \sum_{r=0}^{N} \tilde{E}_{r+\frac{1}{2},j} \cdot l'_{r+\frac{1}{2}}(\xi_i), \\ \left(\frac{\partial \tilde{F}}{\partial \eta} \right)_{i,j} &= \sum_{r=0}^{N} \tilde{F}_{i,r+\frac{1}{2}} \cdot l'_{r+\frac{1}{2}}(\eta_j) \, . \end{aligned} \tag{12}$$

In the present work, the authors use third and fourth-order TVD Runge-Kutta schemes (Shu, 1987) for temporal discretization. Furthermore, for the present test cases, the time-step value is chosen to be small enough so that the error of the solution can be solely attributed to the space discretization scheme and not to the time marching scheme. No special limiter technique is considered for this study, therefore, only flows with smooth initial conditions and solutions are tested. This restriction does not affect the accuracy assessment studies and allows the SD method reconstruction to be applied over the whole computational domain.

3. Accuracy Assessment

The accuracy of the SD method is tested for the linear wave equation,

$$\frac{\partial u}{\partial t} + \frac{\partial u}{\partial x} = 0 \tag{13}$$

for $-1 \leq x \leq 1$ and $u(x,0) = u_0(x)$ with periodic boundary condition at the domain extremes. For this setup, the initial condition is $u_0(x) = \sin(\pi x)$. No limiters are used in this study, given that the solution is smooth. A third-order TVD Runge-Kutta method is employed for time integration with a Δt value of 10^{-4}, in order to make the discretization error time-step independent. Table 1 shows the L_1 and L_∞ error norms produced using the SD method with the Gauss-Lobatto solution point distribution and Fig. 2 plots the solution error versus mesh sizes. Here, NDOF and h denote the number of degrees-of-freedom and a characteristic mesh length, respectively. The error is the difference between the numerical and analytic solutions. One can note that the SD method is able to achieve the expected order of accuracy. However, the performance of the fifth and sixth-order SD scheme is questionable, specially for the finer meshes. This is most likely related to the oscillatory behavior of the polynomial interpolation, due to the internal point distribution chosen. As the grid is refined, the errors actually increase in both norms, which give a negative order of accuracy.

ISSN 2176-5480

Table 1. Accuracy assessment of the 1-D SD method for the wave equation.

Order	NDOF	h	L_∞ error	L_∞ order	L_1 error	L_1 order
2	4	1.000E+00	6.021E-01	–	5.413E-01	–
	8	5.000E-01	4.215E-01	0.51	3.108E-01	0.80
	32	1.250E-01	4.090E-02	1.88	2.578E-02	1.88
	128	3.125E-02	2.618E-03	2.00	1.659E-03	1.99
	512	7.812E-03	1.637E-04	2.00	1.041E-04	2.00
	2048	1.953E-03	1.023E-05	2.00	6.510E-06	2.00
	4096	9.766E-04	2.557E-06	2.00	1.628E-06	2.00
3	6	1.000E+00	3.387E-01	–	2.029E-01	–
	12	5.000E-01	5.234E-02	2.69	1.937E-02	3.39
	48	1.250E-01	5.535E-04	3.27	2.402E-04	3.12
	192	3.125E-02	9.059E-06	2.90	3.634E-06	2.99
	768	7.812E-03	1.480E-07	2.98	5.763E-08	2.99
	3072	1.953E-03	2.338E-09	2.99	9.047E-10	3.00
	6144	9.766E-04	2.928E-10	3.00	1.132E-10	3.00
4	8	1.000E+00	6.080E-02	–	2.709E-02	–
	32	2.500E-01	2.073E-04	3.94	8.377E-05	4.13
	128	6.250E-02	8.314E-07	3.99	3.141E-07	4.01
	512	1.562E-02	3.260E-09	4.00	1.224E-09	4.00
	2048	3.906E-03	1.263E-11	4.01	4.808E-12	3.99
	8192	9.766E-04	5.157E-13	0.57	3.065E-13	0.27
5	10	1.000E+00	9.320E-03	–	3.630E-03	–
	40	2.500E-01	1.153E-05	5.10	6.207E-06	4.86
	160	6.250E-02	1.142E-08	4.97	6.103E-09	5.00
	640	1.562E-02	1.127E-11	4.99	5.982E-12	4.99
	2560	3.906E-03	2.104E-13	1.02	1.298E-13	0.89
	10240	9.766E-04	7.930E-13	-0.99	4.995E-13	-1.00
6	12	1.000E+00	1.672E-03	–	6.279E-04	–
	48	2.500E-01	4.068E-07	5.80	1.415E-07	6.02
	192	6.250E-02	9.464E-11	6.03	3.641E-11	5.98
	768	1.562E-02	1.679E-13	3.10	9.192E-14	2.65
	3072	3.906E-03	6.010E-13	-0.98	3.786E-13	-1.00
	12288	9.766E-04	2.386E-12	-0.99	1.515E-12	-1.00

ISSN 2176-5480

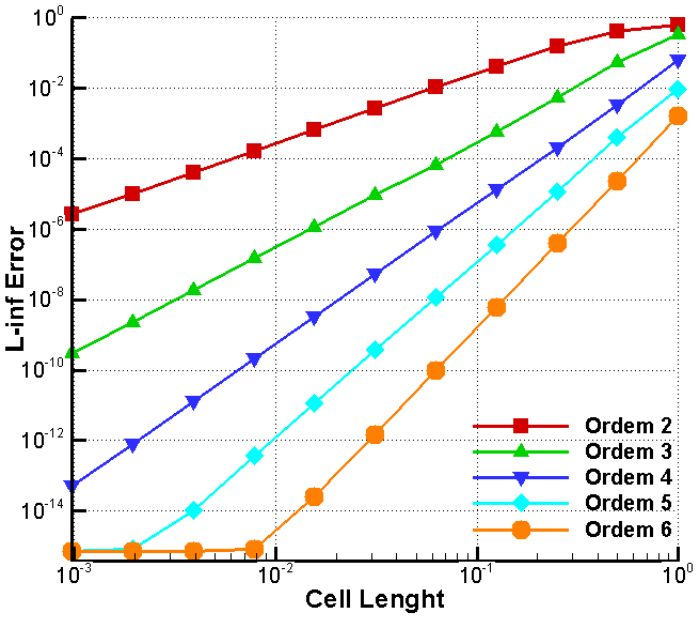

Figure 2. Spectral Difference solution error versus mesh spacing plot order of accuracy measurement of a sine wave convection.

4. Results

The results presented here attempt to verify the stability and resolution of the high-order method for aeronautical applications. For the presented results, density is made dimensionless with respect to the free stream condition and pressure is made dimensionless with respect to the density times the speed of sound squared. Moreover, the L_{max} norm of the residue for the mass equation is used for the convergence history plots. All test cases are executed on an Intel Xeon 2.6 GHz 64-bit Linux computer. The solver is serial, Fortran 90 code with dynamic memory allocation compiled with optimized settings for the Intel compiler.

4.1 Ringleb Flow

The Ringleb flow simulation consists of an internal flow, which has an analytic solution for the Euler equations derived with the hodograph transformation (Shapiro, 1953). The fluid in the domain is initialized as stationary. The flow depends on the inverse of the stream function, k, and the velocity magnitude, v_t. In the present simulations, these parameters are chosen as $k = 0.4$ and $k = 0.6$, in order to define the bounding walls, and $v_t = 0.35$ to define the inlet and outlet boundaries. For such configuration, the test case represents subsonic, irrotational and isentropic flow around a symmetric blunt obstacle. An interesting property of the Ringleb test case is that transition of flow regime, from subsonic to supersonic, for example, is shockless (Wang and Liu, 2006).

Figures 3 presents the various levels of meshes used to solve the Ringleb flow problem. Depending on the order of accuracy, each mesh element in the initial mesh, from Fig. 3(a), is further partitioned to account for the solution and flux points within the mesh, as in Fig. 1. The mesh is composed of quadrilateral elements disposed in a structured way, despite the unstructured mesh treatment by the solver. It should be observed that only half of the Ringleb mesh is shown in these pictures, due to the symmetry of the geometry. Nevertheless, the solution is computed for the whole domain, as the result figures, that follow, demonstrate.

ISSN 2176-5480

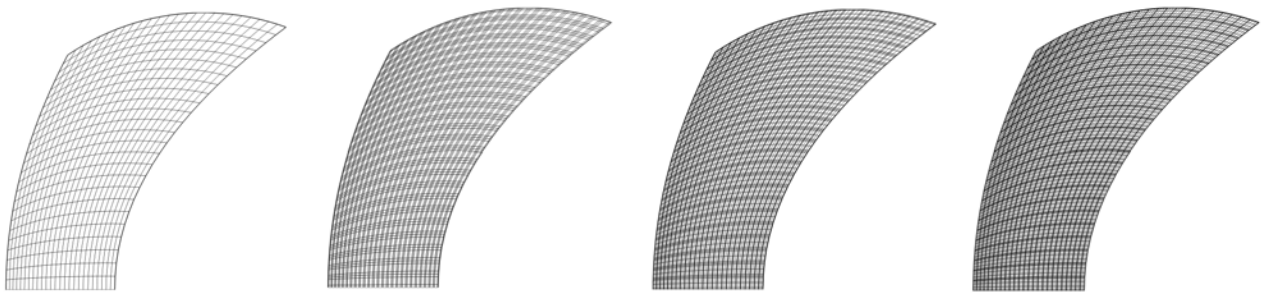

(a) Initial mesh. (b) 2nd-order mesh. (c) 3rd-order mesh. (d) 4th-order mesh.

Figure 3. Meshes for the Ringleb flow problem.

The 2nd, 3rd and 4th-order SD methods are used to compute the solution for this problem. Figure 4 shows the convergence history for all the orders considered. One can observe that a large number of iterations is required for the problem, due to the reduced value of the time-step. Furthermore, stability requirements reduced even further the convergence rate of the 3rd and 4th-order methods. The overall behavior of the residue curves, for the 3rd and 4th-order schemes, indicate that, given enough time, they might converge to machine precision, as the 2nd-order simulation did. Even though the authors considered over 2.5 million iterations for the 3rd-order scheme, a residue magnitude reduction of only 3 and 5 orders, for the 4th and 3rd order methods respectively, is observed. In any event, such residue levels should not compromise the resulting analyses, considering that the maximum-norm of the residue is monitored and shows no indication that any simulation could diverge.

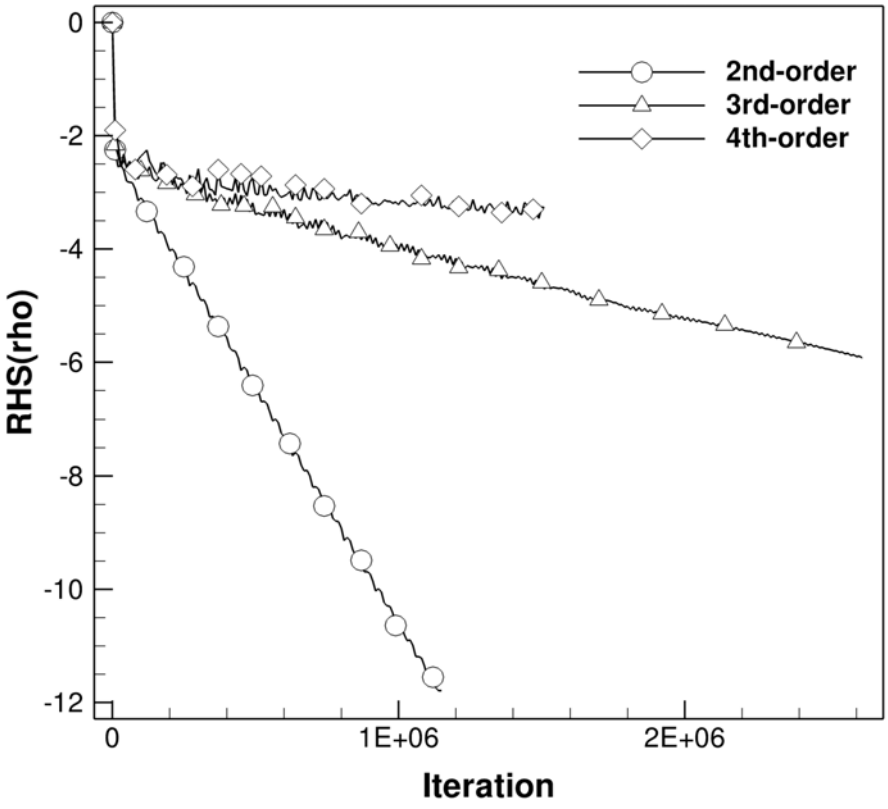

Figure 4. Ringleb flow problem convergence history.

Figures 5 and 6 presents pressure and Mach number contours, respectively. The pressure contours range from 0.55 to 0.81 with twenty levels. The Mach number contours range from 0.25 to 0.8 in nine equally spaced levels. With regard to the pressure contours, one can note that the 4th-order scheme presents smoother contours, particularly near the left and right walls. It should be mentioned that such oscillations might be associated with the technique used to interpolate the solution to the high-order mesh for visualization. Furthermore, the structured topology of the mesh might contribute to such behavior. Further investigations are being conduct with different mesh topologies and orders of the SD scheme to verify these questions. A second comment, regarding the flow properties contours, is that the solution is not symmetric,

ISSN 2176-5480

even for the converged 2nd-order case. The authors are currently investigating this issue. It is important to note that no effort has been taken, at the time of the writing of this article, to consider curved boundaries on the domain bounding walls (Wang and Liu, 2006). The authors are aware that such condition may introduce errors to the spacial discretization scheme near boundaries, reduce the order of the method and possibly cause instabilities and divergence of the solution.

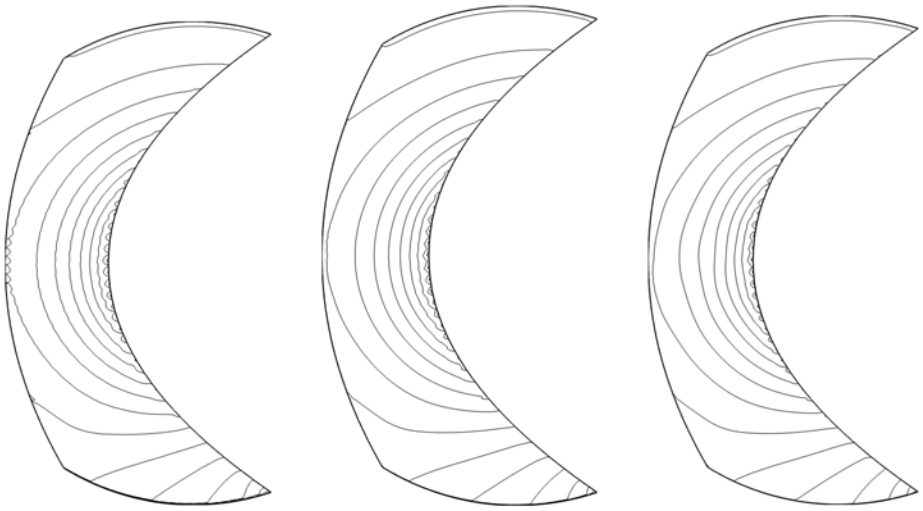

(a) 2nd-order. (b) 3rd-order. (c) 4th-order.

Figure 5. Pressure contours for the Ringleb flow problem.

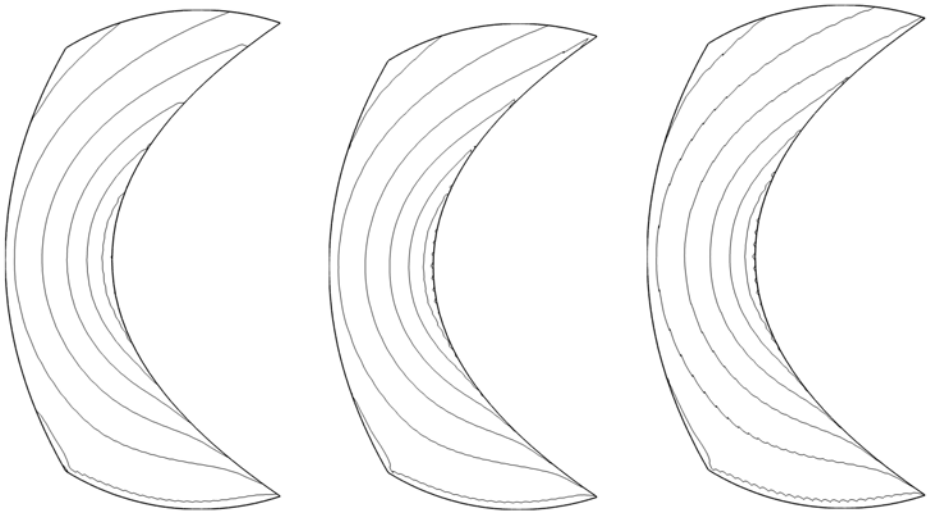

(a) 2nd-order. (b) 3rd-order. (c) 4th-order.

Figure 6. Mach contours for the Ringleb flow problem.

4.2 NACA 0012 Airfoil

A simulation with the NACA 0012 airfoil is considered for the SD method. The Euler equations are solved on a mesh with 10608 cells and 10845 nodes. The symmetry condition is applied to the mesh, due to the geometry and flow conditions for this test case. The far-filed boundary is located at a distance of 10 chords to the airfoil, using an *O*-grid topology. The computational domain is mirrored, for visualizations purposes, in the results figures that follows. The free stream Mach number value of $M_\infty = 0.6$ and $\alpha = 0$ deg. angle-of-attack are used. These conditions ensure a smooth flow throughout the domain. Simulations with the second, third and fourth order SD schemes are performed. Figure 7 presents the several mesh levels for this test case. The initial mesh elements, in Fig. 7(a), are further partitioned to include the solution and flux points for the SD method. The high-order meshes are also used to interpolate the high-order solution for visualization.

ISSN 2176-5480

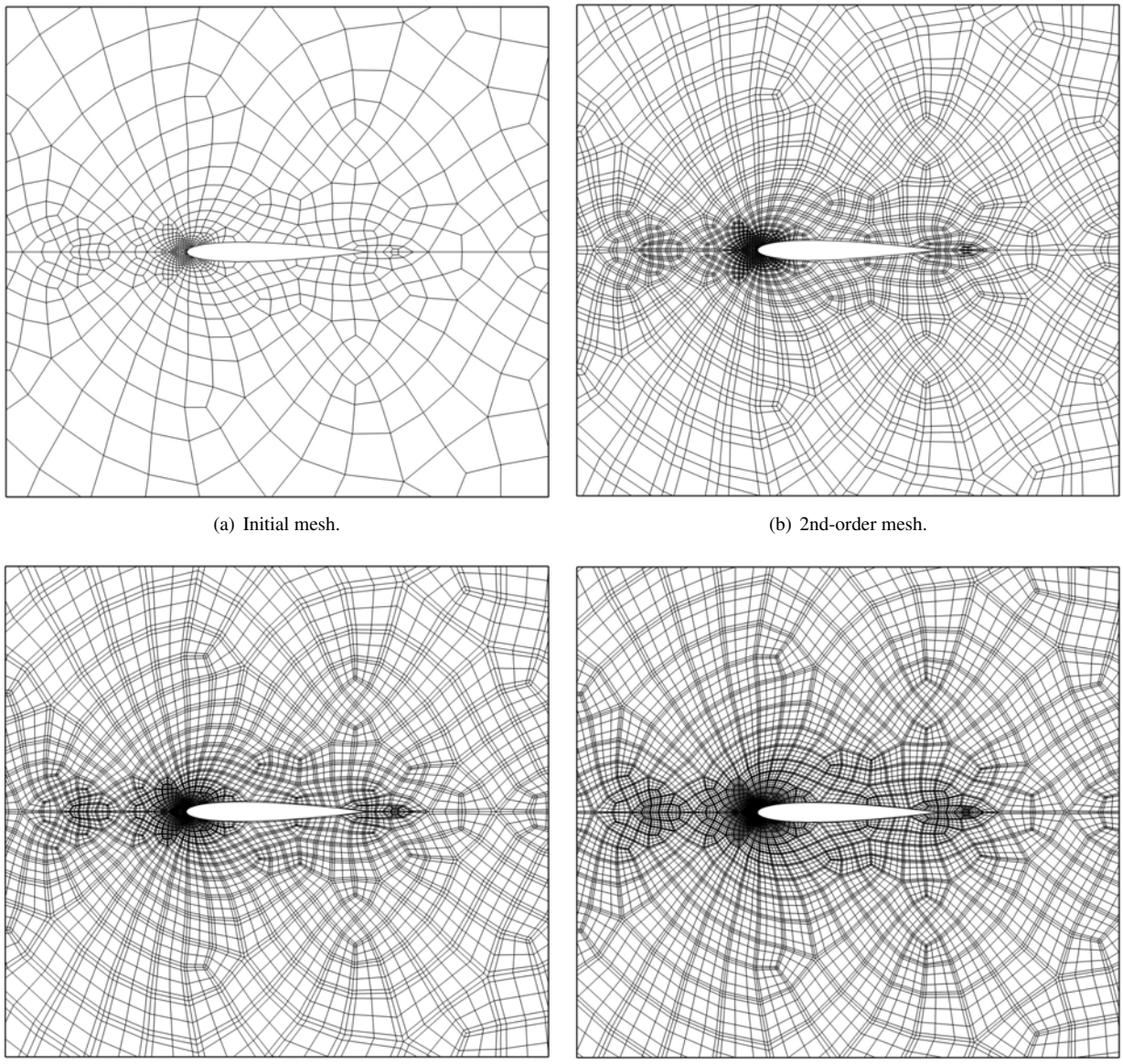

(a) Initial mesh. (b) 2nd-order mesh.

(c) 3rd-order mesh. (d) 4th-order mesh.

Figure 7. Meshes for the NACA 0012 airfoil simulation.

Figure 8 shows the convergence history for all the orders considered for this test-case. Every simulation converged to machine precision, albeit at different convergence rates. The 2nd-order simulation converged at nearly 20,000 iterations, the 3rd-order simulation at 40,000 and the 4th-order case at over 70,000 iterations. This behavior is expected due to the limited CFD value required for numerical stability of high-order schemes (May *et al.*, 2010). In accordance with the previous test case, future studies will consider the analysis of an implicit time-marching scheme coupled to the SD method, which should considerably improve the convergence rate for the high-order simulations.

ISSN 2176-5480

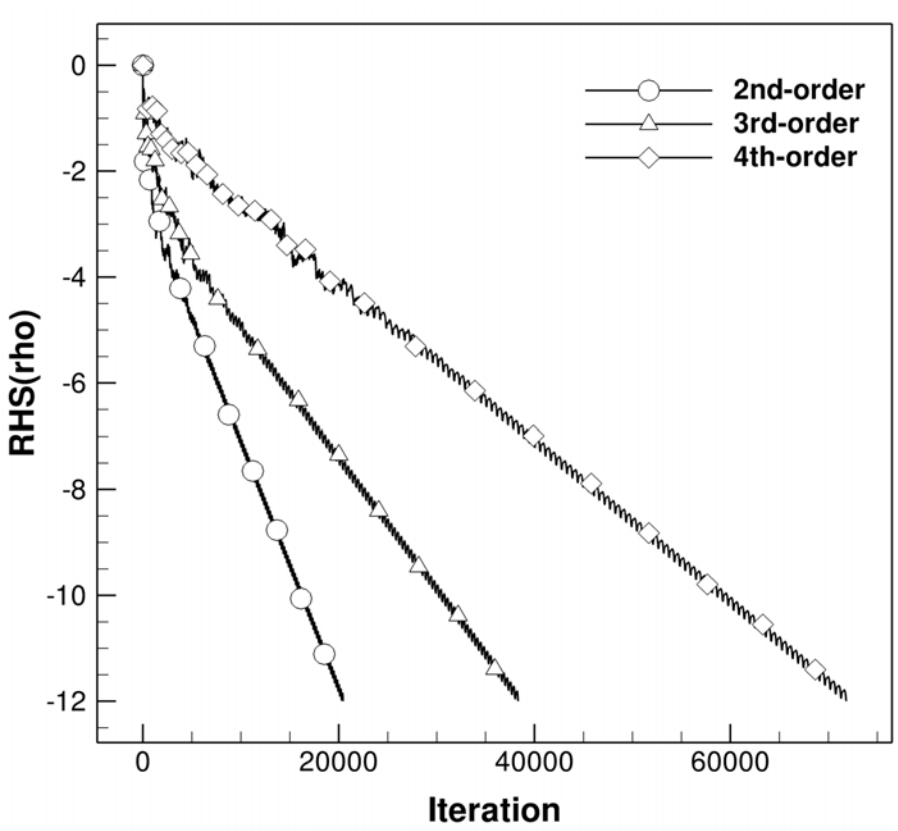

Figure 8. NACA 0012 convergence history.

Figures 9 and 10 show the density and pressure contours for the NACA 0012 airfoil simulations. The flow properties contours share the same color map range and number of levels. Hence, a qualitative comparison can be made from the solutions at different orders of accuracy. One can observe, for the density contours, that a similar behavior to the Ringleb flow problem is observed. That is, the 3rd- and 4th-order solutions are smoother than the 2nd-order scheme. The same comment is valid for the pressure field. Again, it should be mentioned that the airfoil boundaries are represented by linear triangles. No attempt at this time has been taken to include high-order mesh elements in the simulation. It is hard to distinguish the 4th-order solution from the 3rd-order. This might be explained by the fact that, near the airfoil walls, the 4th-order SD method might actually reduce to 3rd- or even 2nd-order accuracy due to the linear triangular elements. Further extensions are in place to include curved boundaries to the solver, for quadratic and cubic reconstructions.

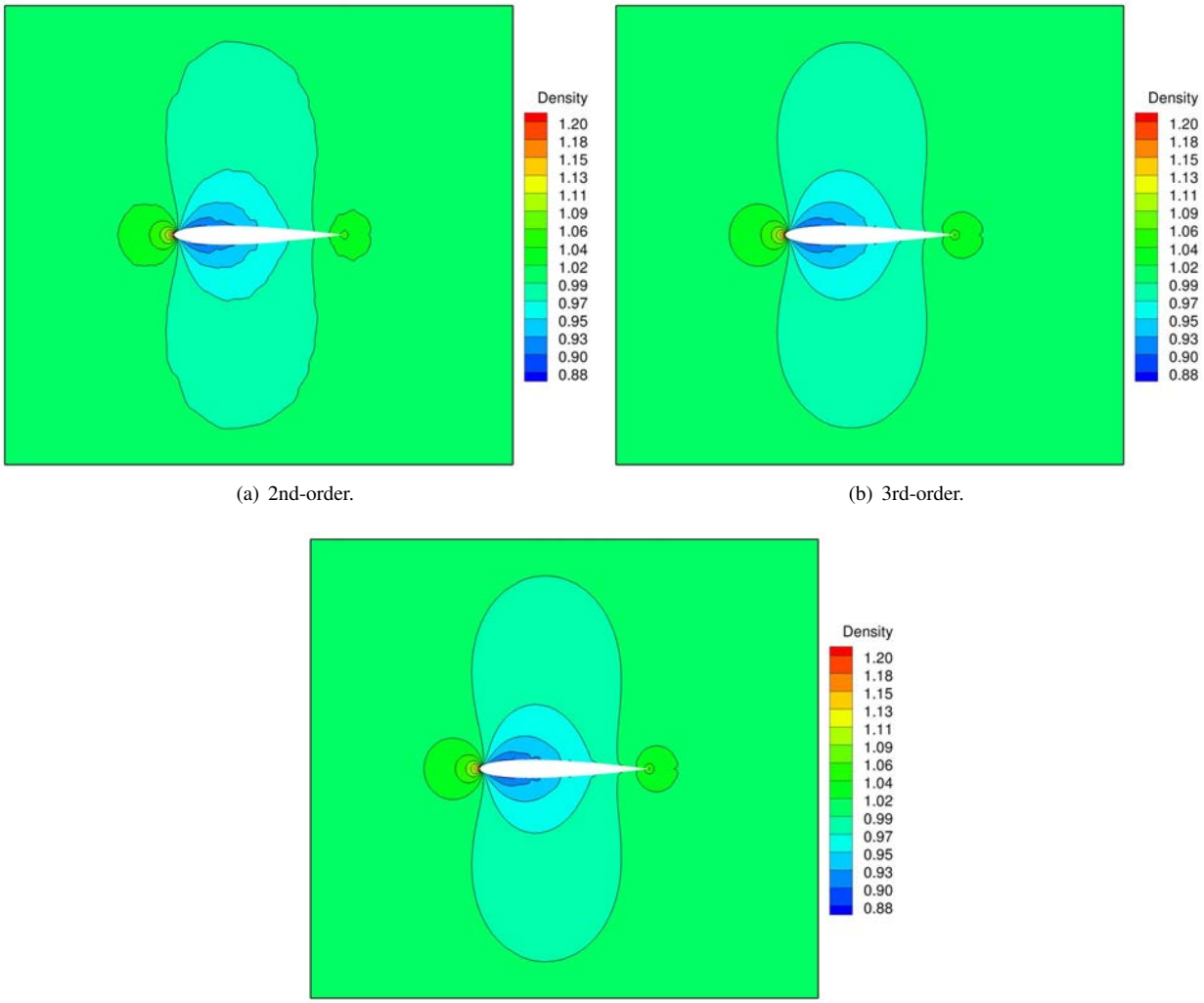

(a) 2nd-order.

(b) 3rd-order.

(c) 4th-order.

Figure 9. Density contours for the NACA 0012 airfoil simulations at $M_\infty = 0.6$ and $\alpha = 0$ deg.

ISSN 2176-5480

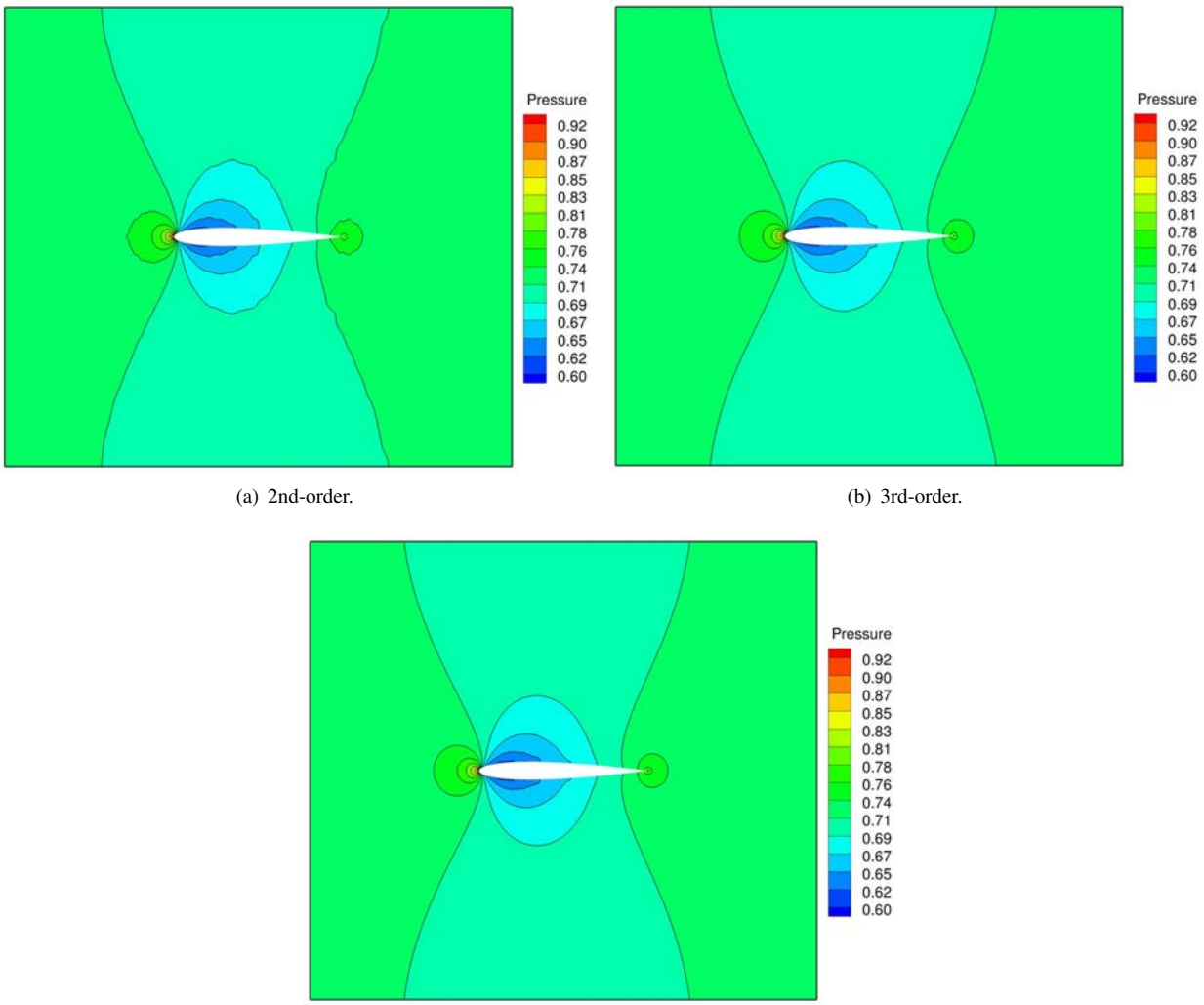

(a) 2nd-order.

(b) 3rd-order.

(c) 4th-order.

Figure 10. Pressure contours for the NACA 0012 airfoil simulations at $M_\infty = 0.6$ and $\alpha = 0$ deg.

ISSN 2176-5480

5. CONCLUDING REMARKS

The present work evaluates the Spectral Difference method for aerodynamic applications. Accuracy studies were performed to measure the formal order of accuracy of the scheme with literature test cases. It is observed that further extensions are necessary to apply the method to a broader class of compressible problems. The proper treatment of discontinuities in the numerical solution and of curved boundary representations are an example. Nevertheless, the present results indicate that the SD method is able to achieve formal order of accuracy for smooth flows and that high-order solutions have the potential to reduce simulation time by employing coarser meshes in comparison to 2nd-order schemes.

6. ACKNOWLEDGEMENTS

The authors gratefully acknowledge the partial support for this research provided by Conselho Nacional de Desenvolvimento Científico e Tecnológico, CNPq, under the Research Grants No. 312064/2006-3 and No. 471592/2011-0. This work is also supported by Fundação Coordenação de Aperfeiçoamento de Pessoal de Nível Superior, CAPES, through a Ph.D. Scholarship for the second author. The authors are also indebted to the partial financial support received from Fundação de Amparo à Pesquisa do Estado de São Paulo, FAPESP, under Grant No. 2013/07375-0.

7. REFERENCES

Breviglieri, C. and Azevedo, J.L.F., 2012. "Unsteady aerodynamic applications using high-order unstructured grid methods". In AIAA Paper No. 2012-0701*, 50th AIAA Aerospace Sciences Meeting Including the New Horizons Forum and Aerospace Exposition*. Nashville, TN.

Breviglieri, C., Azevedo, J.L.F., Basso, E. and Souza, M.A.F., 2010. "Implicit high-order spectral finite volume method for inviscid compressible flows". *AIAA Journal*, Vol. 48, No. 10, pp. 2365–2376.

Liu, Y., Vinokur, M. and Wang, Z.J., 2006. "Spectral difference method for unstructured grids I: Basic formulation". *Journal of Computational Physics*, Vol. 216, pp. 780–801.

May, G., Iacono, F. and Jameson, A., 2010. "A hybrid multilevel method for high-order discretization of the Euler equations on unstructured meshes". *Journal of Computational Physics*, Vol. 229, No. 10, pp. 3938–3956.

May, G. and Jameson, A., 2006. "A spectral difference method for the Euler and Navier-Stokes equations on unstructured meshes". In *44th AIAA Aerospace Sciences Meeting*. AIAA Paper No. 2006-304, Reno, NV.

Shapiro, A.H., 1953. *The Dynamics and Thermodynamics of Compressible Fluid Flow*. Wiley, New York.

Shu, W.C., 1987. "TVB uniformly high-order schemes for conservation laws". *Mathematics of Computation*, Vol. 49, pp. 105–121.

Wang, Z.J., 2002. "Spectral (finite) volume method for conservation laws on unstructured grids: Basic formulation". *Journal of Computational Physics*, Vol. 178, No. 1, pp. 210–251.

Wang, Z.J. and Liu, Y., 2006. "Extension of the spectral volume method to high-order boundary representation". *Journal of Computational Physics*, Vol. 211, No. 1, pp. 154–178.

Wang, Z.J., Liu, Y., May, G. and Jameson, A., 2007. "Spectral difference method for unstructured grids II: Extension to the Euler equations". *Journal of Scientific Computing*, Vol. 32, No. 1.

8. RESPONSIBILITY NOTICE

The authors are the only responsible for the printed material included in this paper.